Compressing and focusing a short laser pulse by a thin plasma lens

C. Ren,[1] B. J. Duda,[1] R. G. Hemker,[1] W. B. Mori,[1] T. Katsouleas,[2]
T. M. Antonsen, Jr.,[3] and P. Mora[4]
[1]*University of California, Los Angeles, Los Angeles, California 90095-9000*
[2]*University of Southern California, Los Angeles, California 90089-0484*
[3]*University of Maryland, College Park, Maryland 20742*
[4]*Centre de Physique Theorique, Ecole Polytechnique, Palaiseau, France*
(Received 8 June 2000; published 25 January 2001)

We consider the possibility of using a thin plasma slab as an optical element to both focus and compress an intense laser pulse. By thin we mean that the focal length is larger than the lens thickness. We derive analytic formulas for the spot size and pulse length evolution of a short laser pulse propagating through a thin uniform plasma lens. The formulas are compared to simulation results from two types of particle-in-cell code. The simulations give a greater final spot size and a shorter focal length than the analytic formulas. The difference arises from spherical aberrations in the lens which lead to the generation of higher-order vacuum Gaussian modes. The simulations also show that Raman side scattering can develop. A thin lens experiment could provide unequivocal evidence of relativistic self-focusing.

DOI: 10.1103/PhysRevE.63.026411 PACS number(s): 52.35.Mw, 52.38.−r

I. INTRODUCTION

Studying intense laser pulse propagation in plasmas is important to many applications including laser fusion, laser plasma acceleration [1], and plasma-based light sources [2]. At high laser intensities nonlinear interactions between the plasma and the laser become important. One fundamental nonlinear effect arises from the relativistic motion of the electrons in the intense laser field [3]. In particular, the laser pulse's transverse and axial dimensions can be changed by relativistic self-focusing (RSF) [4–9] and relativistic self-phase modulation (RSPM) [5,10]. In RSF the transverse spot size can decrease when a transverse gradient of the index of refraction causes the wave fronts to curve so that energy is focused radially inward. In RSPM the laser pulse length can be compressed by a frequency chirp that is induced by the nonlinear dependence of the axial phase velocity. This leads to an axial chirp of the group velocity where the back of the pulse moves faster (higher frequency) and the front of the pulse moves more slowly (lower frequency), causing the pulse to compress. The pulse focusing and compressing are dynamically related through the change of the pulse intensity.

While relativistic self-focusing was theoretically predicted more than 25 years ago [4], in a strict sense it has yet to be unequivocally demonstrated in a laboratory experiment. All relevant experiments to date [11] have provided clear evidence that a laser could propagate for distances exceeding the vacuum diffraction length. These experiments have therefore shown optical guiding, but they have not unequivocally shown a spot size reduction when the power roughly exceeded a critical power or an intensity enhancement. The difficulty arises because in each experiment the plasma length greatly exceeded both the Rayleigh and self-focusing lengths. Therefore, the pulse rapidly self-focuses within the plasma and violently goes unstable to stimulated Raman forward scattering [12] and this greatly complicates the interpretation.

In this paper, we propose using a plasma as a thin lens for focusing high-intensity lasers. In this thin lens concept the laser pulse receives an impulsive focusing force while in the plasma, and then focuses well outside the plasma in the vacuum region. As such it may be a means of carrying out an unequivocal demonstration of relativistic self-focusing. Moreover, it may prove to be a simple alternative to conventional optics, which may be subject to damage by very high-intensity lasers. In this sense it is the optical analogy to the well known plasma lens for particle beams [13,14]. To study the thin lens concept, we use the particle-in-cell (PIC) codes WAKE [15] and OSIRIS [16]. The simulation parameters were chosen to model a short pulse passing through a thin plasma with a thickness of a few percent of the vacuum Rayleigh length.

The paper is organized as follows. In Sec. II we derive analytical formulas for the simultaneous evolution of spot size and pulse length. To our knowledge, this is the first time that an equation for the evolution of the pulse length has been derived. We use these formulas to derive the focal length and spot size reduction for an idealized thin lens. In Sec. III simulation results are presented and the results are compared to the analytical results. The paper is summarized in Sec. IV.

II. ANALYTICAL ANALYSIS

To derive formulas for the spot size and pulse length evolution, we start from the equation of the laser vector potential in the plasma using only the relativistic nonlinearity,

$$\left(\nabla_\perp^2+\frac{\partial^2}{\partial z^2}-\frac{1}{c^2}\frac{\partial^2}{\partial t^2}\right)\tilde{A}=\frac{\omega_p^2}{c^2}\left(1-\frac{\tilde{A}^2}{2}\right)\tilde{A}, \qquad (2.1)$$

where $\tilde{A}$ is the vector potential normalized to mc^2/e, ω_p is the plasma frequency, and c is the speed of light. The nonlinearity is approximated by $\tilde{A}^2/2$ and the plasma wave wake is ignored to make the problem analytically tractable. By neglecting the wake we preclude Raman type instabilities

from the analysis. First we write $\tilde{A}$ as the product of an envelope and a phase, $\tilde{A}=ae^{-i(\omega_0 t-k_0 z)}/2+\text{c.c.}$, where ω_0 and k_0 satisfy the linear dispersion relation $\omega_0^2=k_0^2c^2+\omega_p^2$. We then make a mathematical transformation from the coordinate variables (t,z) to variables (τ,ψ) where $\tau=z$ and $\psi=t-z/v_g$; note that in nonlinear optics a wave equation for electric field E is used while in short pulse laser-plasma interaction an equation for $\tilde{A}$ is used [17,18]. The equation for the envelope a now becomes

$$2ik_0\frac{\partial a}{\partial\tau}+\left(\frac{1}{v_g^2}-\frac{1}{c^2}\right)\frac{\partial^2 a}{\partial\psi^2}-\frac{2}{v_g}\frac{\partial^2 a}{\partial\psi\partial\tau}+\nabla_\perp^2 a+\frac{\omega_p^2}{c^2}\frac{|a|^2}{4}a=\left(\frac{2i\omega_0}{c^2}-\frac{2ik_0}{v_g}\right)\frac{\partial a}{\partial\psi}+\frac{\partial^2 a}{\partial\tau^2}. \tag{2.2}$$

We choose v_g to be the linear group velocity, $v_g=k_0c^2/\omega_0$. We also assume the second terms on the right side of the above equation is much smaller when compared with the other terms. Thus, the right side is zero.

The second and third term on the left side of Eq. (2.2) represent some of the finite pulse length effects. The second term is called the group velocity dispersion term and at low intensity leads to pulse broadening. However, this term in combination with the nonlinear term can lead to pulse compression as well as self-phase modulational instabilities. The third term causes pulse self-steepening, nonlinear corrections to the group velocity, and higher-order corrections to the growth rate for RSPM. We have developed a general perturbation method of treating this term and the result will be reported in a separate paper. The fourth term leads to diffraction and needs to be kept when studying self-focusing. There has also been some recent work on lasers propagating in channels which also addresses some of these issues [19,20].

Therefore, the simplest equation that includes both compression and self-focusing is

$$2ik_0\frac{\partial a}{\partial\tau}+\frac{\epsilon^2}{c^2}\frac{\partial^2 a}{\partial\psi^2}+\nabla_\perp^2 a+\frac{\omega_p^2}{c^2}\frac{|a|^2}{4}a=0, \tag{2.3}$$

where $\epsilon\equiv\omega_p/k_0c$. This equation can be approximately solved using a variational principle, just as in the case of self-focusing alone [21–23]. We begin by writing down the Lagrangian density for Eq. (2.3), which can be shown to be

$$\mathcal{L}=ik_0\left(a\frac{\partial a^*}{\partial\tau}-a^*\frac{\partial a}{\partial\tau}\right)+\frac{\epsilon^2}{c^2}\frac{\partial a^*}{\partial\psi}\frac{\partial a}{\partial\psi}+\nabla_\perp a^*\cdot\nabla_\perp a-\frac{\omega_p^2}{c^2}\frac{a^2a^{*2}}{8}, \tag{2.4}$$

i.e., Eq. (2.3) is the Euler-Lagrange equation for minimizing the action $S=\int d\tau d\vec{x}_\perp d\psi\mathcal{L}$ for variations in a^* (and a).

Next we use the following trial function:

$$a=\frac{A(\tau)}{W(\tau)\sqrt{L(\tau)}}e^{-i\phi(\tau)}e^{i\psi^2/\eta(\tau)}e^{-\psi^2/L^2}e^{ik_0r^2/2R(\tau)}e^{-r^2/W^2}. \tag{2.5}$$

Here, the pulse length L, spot size W, amplitude A, phase ϕ, chirp η, and radius of curvature R are all real. Substituting this trial function into Eq. (2.4) and integrating in ψ and $\vec{x}_\perp$, we obtain a reduced Lagrangian density

$$\begin{aligned}\bar{\mathcal{L}}&\equiv\frac{1}{4\sqrt{\pi}}\int_0^\infty r\,dr\int_{-\infty}^\infty d\psi\mathcal{L}\\&=-\sqrt{2}k_0A^2\left(\frac{d\phi}{d\tau}+\frac{L^2}{4\eta^2}\frac{d\eta}{d\tau}+\frac{k_0W^2}{4R^2}\frac{dR}{d\tau}\right)+\frac{\epsilon^2}{c^2}\frac{A^2}{\sqrt{2}}\left(\frac{1}{L^2}+\frac{L^2}{\eta^2}\right)+\frac{A^2}{\sqrt{2}}\left(\frac{2}{W^2}+\frac{k_0^2W^2}{2R^2}\right)\\&\quad-\frac{\omega_p^2}{c^2}\frac{A^4}{32W^2L}.\end{aligned} \tag{2.6}$$

Next, we use the Euler-Lagrange equations of the reduced Lagrangian density to derive the evolution of W and L in τ.

A. An idealized thin lens: Spot size evolution

We consider the ideal case where a thin plasma lens with a thickness Δ is placed at the vacuum waist $(\tau=0)$ of a Gaussian laser pulse with a spot size W_0. The laser exits the plasma at $\tau=\Delta$ and reaches its focus, where it has a minimum spot size W_{min}, at $\tau=f$. We study how W_{min} and f depend on Δ and the normalized laser power P/P_c, where $P_c\equiv17\omega_0^2/\omega_p^2$ GW is the critical power for RSF [7].

If the pulse is assumed to remain Gaussian and finite pulse length effects are neglected, i.e., L and η are assumed to remain fixed, then the evolution equation for the spot size W inside the plasma can be derived from the reduced Lagrangian Eq. (2.6). Varying ϕ leads to power conservation,

$$\frac{dA^2}{d\tau}=0. \tag{2.7}$$

Varying R relates R and $dW/d\tau$,

$$\frac{W}{R}=\frac{dW}{d\tau}. \tag{2.8}$$

Varying W gives another equation for R and W,

$$-\frac{k_0^2}{\sqrt{2}}\frac{A^2W}{R^2}\frac{dR}{d\tau}+\frac{A^2}{\sqrt{2}}\left(\frac{-4}{W^3}+\frac{k_0^2W}{R^2}\right)+\frac{\omega_p^2}{c^2}\frac{A^4}{16W^3L}=0. \tag{2.9}$$

Substituting Eq. (2.8) into Eq. (2.9) to eliminate R, we obtain the evolution equation for the spot size W [24],

$$\frac{d^2W}{d\tau^2} = -\frac{4}{k_0^2 W^3}\left(\frac{P}{P_c} - 1\right), \tag{2.10}$$

where $P/P_c \equiv \sqrt{2}A^2\omega_p^2/(64c^2L)$ is independent of τ. Identical equations for RSF can be obtained via other means, most notably the source dependent expansion [25]. Note that if our trial function was an infinitely long pulse then $P/P_c \equiv A^2\omega_p^2/(32c^2)$, which is the often quoted result. This is probably more accurate for the spot size of the peak.

The solution to Eq. (2.10), with the initial condition of $W = W_0$ and $dW/d\tau = 0$ at $\tau = 0$, is

$$W = W_0\sqrt{1 - \left(\frac{P}{P_c} - 1\right)\left(\frac{\tau}{\tau_R}\right)^2}, \tag{2.11}$$

where $\tau_R \equiv k_0 w_0^2/2$ is the vacuum Rayleigh length for the laser pulse. Equation (2.11) predicts that the spot size will eventually go to zero if $P/P_c > 1$. In reality, spot size collapse is prevented by higher-order relativistic terms and electron cavitation [7,8]. For the thin plasma lens case where the pulse is focused only slightly within the plasma, this solution can describe the spot size evolution well. The spot size at the exit of the lens is $W_{exit} = W_0\sqrt{1-\delta^2}$, where

$$\delta \equiv (\Delta/z_R)\sqrt{(P/P_c - 1)}$$

is the normalized lens thickness.

When the laser exits the plasma, the spot size evolves as

$$\frac{d^2W}{d\tau^2} = \frac{4}{k_0^2 W^3}, \tag{2.12}$$

which has a solution

$$W = W_{min}\sqrt{1 + \left(\frac{\tau - f}{\tau_R}\right)^2 \frac{W_0^4}{W_{min}^4}}. \tag{2.13}$$

By matching W and dW/dz from Eqs. (2.11) and (2.13) at $\tau = \Delta$, we can determine the minimum spot size W_{min} and focal length f:

$$W_{min} = W_0\sqrt{\frac{1-\delta^2}{1 + (P/P_c - 1)\delta^2}}, \tag{2.14}$$

$$f = \Delta\frac{P/P_c}{1 + (P/P_c - 1)\delta^2}. \tag{2.15}$$

To get a lens design for $W_{min}/W_0 \ll 1$ and $f/\Delta \gg 1$, a high laser power is needed. In the limit of $\delta^2 P/P_c \gg 1$, simplified expressions for W_{min} and f can be obtained:

$$W_{min} \approx \frac{W_0}{\sqrt{P/P_c\,\delta^2}}, \tag{2.16}$$

$$f \approx \frac{\Delta}{\delta^2}. \tag{2.17}$$

B. Pulse length evolution

In this section, we consider how the pulse length evolves in the idealized case where the spot size remains constant in τ at each axial position. From Eq. (2.6), we vary the independent variables ϕ, η, L, and A to determine their τ dependence while keeping W and R fixed. Varying ϕ leads to power conservation,

$$\frac{dA^2}{d\tau} = 0. \tag{2.18}$$

Varying η relates η and $dL/d\tau$,

$$\frac{1}{\eta} = \frac{k_0 c^2}{2\epsilon^2 L}\frac{dL}{d\tau}. \tag{2.19}$$

Varying L gives another equation for η and L,

$$-\frac{k_0}{\sqrt{2}}\frac{A^2 L}{\eta^2}\frac{d\eta}{d\tau} + \frac{\epsilon^2}{c^2}\frac{A^2}{\sqrt{2}}\left(\frac{-2}{L^3} + \frac{2L}{\eta^2}\right) + \frac{\omega_p^2}{c^2}\frac{A^4}{32W^2L^2} = 0. \tag{2.20}$$

Substituting Eq. (2.19) into Eq. (2.20) to eliminate η, we obtain the evolution equation for the pulse length L,

$$\frac{d^2L}{d\tau^2} = -\frac{\epsilon^4}{c^4}\frac{4}{k_0^2 L^3}\left(\frac{\sqrt{2}A^2\omega_p^2}{64W^2\epsilon^2}L - 1\right). \tag{2.21}$$

We note that here L has a unit of time, not length. Therefore, the distance required for pulse compression scales as $k_0 L^2 c^2/2\epsilon^2$. For a high-intensity laser pulse, where $\sqrt{2}A^2\omega_p^2 L/(64\epsilon^2) \gg 1$, Eq. (2.21) can be solved analytically to obtain

$$\frac{\epsilon^2 a_0}{2^{5/4}}\frac{\tau}{cL_0} = \frac{\sqrt{L_0/L - 1}}{L_0/L} + \arctan\sqrt{L_0/L - 1}, \tag{2.22}$$

where a_0 and L_0 are the initial normalized vector potential and pulse length, respectively. When inverted, this transcendental equation gives $L(\tau)$. Later, we solve it numerically to compare to the simulation results.

C. Simultaneous self-focusing and compression

In the previous subsections we derived decoupled envelope equations for the evolution of spot size and pulse length while the other was held fixed. We did this to clearly illustrate each process. We now obtain coupled equations to consider how self-focusing can accelerate the pulse compression rate. We emphasize that these equations are idealized since they assume that one spot size describes the beam at any instant of τ. In reality the spot size will also depend on ψ, but this makes the analysis much more complicated and makes integrating the action over ψ intractable.

It turns out that the coupled equations for L and W have exactly the same form as Eqs. (2.10) and (2.21), only now both L and W are functions of τ. We write these two equations in the following form to emphasize the coupling between L and W:

TABLE I. Simulation summary.

P_0/P_c	L_{FWHM} (fs)	Δ (mm)	$f-\Delta$ (mm)	W_{min}/W_0	L_{min}/L_0	$(a_{max}/a_0)^2$	P_{max}/P_0	$(W_{min}/W_0)_{theor}$	$(L_{min}/L_0)_{theor}$
100	57	1.0	3.4	0.68	0.97	19	1.1	0.29	0.96
100	45	1.6	0.43	0.60	0.92	231	1.8	0.16	0.85
100	45	1.0	3.4	0.64	0.98	28	1.4	0.29	0.93
11	45	0.7	0.33	0.75	1	23	1.0	0.35	0.96

$$\frac{d^2W}{d\tau^2}=-\frac{4}{k_0^2W^3}\left(\frac{L_c}{L}-1\right) \tag{2.23}$$

and

$$\frac{d^2L}{d\tau^2}=-\frac{\epsilon^4}{c^4}\frac{4}{k_0^2L^3}\left(\frac{L_cL}{W^2}\frac{c^2}{\epsilon^2}-1\right), \tag{2.24}$$

where $L_c\equiv\sqrt{2}A^2\omega_p^2/(64c^2)$ is a constant. These coupled equations show that, if $L<L_c$ (i.e., $P>P_c$), then W decreases from self-focusing. At the same time the pulse compressing rate increases, scaling as W^{-2}. Thus, as an intense pulse propagates, focusing and compressing reinforce each other. For completeness, we notice that there is a first integral for the coupled Eqs. (2.23) and (2.24),

$$\frac{1}{2}(c^2\dot{L}^2+2\epsilon^2\dot{W}^2)+\frac{4}{k_0^2}\left[\frac{\epsilon^2}{W^2}\left(1-\frac{L_c}{L}\right)+\frac{\epsilon^4}{2c^2L^2}\right]=\text{const.} \tag{2.25}$$

This can be obtained either by examining Eqs. (2.23) and (2.24) or from obtaining the Hamiltonian from the reduced Lagrangian.

D. Importance of Raman scattering

In the analysis just presented of a thin lens concept only the relativistic nonlinearity was included. However, in many instances Raman forward scattering (RFS) will occur and this will compete with the self-focusing process. While including RFS into the analytical framework is beyond the scope of this work we can estimate its importance by using known expressions for the amount of RFS exponentiation. Basically, there are three regimes of RFS growth that are important. These are RFS, four-wave nonresonant RFS–side scattering (RFS-SS), and three-wave RFS-SS [26]. In terms of laser power P/P_c, lens thickness Δ, and pulse length L, the gains (number of *e*-foldings) for these instabilities can be written as [26]

$$G=\sqrt{8\epsilon\frac{P}{P_c}\frac{\Delta}{\tau_R}\frac{L\omega_p}{c}}, \quad \text{RFS}, \tag{2.26}$$

$$G=1.64\sqrt[3]{\frac{P}{P_c}\left(\frac{\Delta}{\tau_R}\right)^2\frac{L\omega_p}{c}},$$

four-wave nonresonant RFS-*SS* $(k_\perp W=1)$, (2.27)

and

$$G=2\sqrt{\frac{P}{P_c}\frac{\Delta}{\tau_R}\frac{L\omega_p}{c}}, \quad \text{three-wave RFS-SS}. \tag{2.28}$$

The most important one for the thin lens concept is the RFS-SS. This can be seen by rewriting Eq. (2.28) in terms of spot size reduction using Eq. (2.16),

$$G=2\sqrt{\frac{W_0}{W_{min}}\frac{L\omega_p}{c}}. \tag{2.29}$$

This means $G\approx 9$ for a pulse length of one plasma wavelength $(L\omega_p/c=2\pi)$ to reach a spot size reduction of $W_0/W_{min}=3$.

III. SIMULATION RESULTS

A. Comparing spot size and pulse length with theory

To study the viability of a thin lens concept, we use the particle-in-cell codes WAKE [15] and OSIRIS [16]. The code WAKE simulates the evolution of the laser field and plasma on a time scale much greater than the laser oscillation period. The laser field is described by its envelope equation which is derived by averaging the wave equation over the fast laser oscillation frequency. The particles move under the laser ponderomotive force and the self-consistent field. On the other hand, OSIRIS is a fully parallelized, fully explicit PIC code which resolves the entire laser oscillation.

We did a series of simulations using WAKE in cylindrically symmetric geometry to understand the limitations of the thin lens scaling laws. The parameters were chosen so that W_0/W_{min} and f/Δ were predicted to be large. A representative set of simulation parameters is shown in Table I where the laser wavelength is assumed to be 1 μm. In each case the laser was focused to the edge of the lens with an incident normalized vector potential of $a_0=1$ and a lens density of $n_e=10^{19}$ cm^{-3}, while in most cases the spot size was $W_0=100$ μm so that the laser power was 170 TW. For these values the normalized parameters correspond to $\epsilon\equiv\omega_p/\omega_0=0.09$, $P/P_c=100$, and $W_0=57c/\omega_p$. For the $P/P_c=11$ case, $W_0=19c/\omega_p$, and the laser power is 19 TW. In the simulations the laser pulse length L_0 and the lens thickness Δ were varied.

For illustrative purposes, we begin by presenting results from a simulation in which $L_0=7.52c/\omega_p$, corresponding to a full width at half maximum pulse length $L_{\mathrm{FWHM}}=57$ fs and $\Delta=0.0316z_R$ (1 mm). Under these conditions Eqs. (2.14) and (2.15) predict $W_{min}=0.3W_0$ and $f=10\Delta$.

In Fig. 1 the theoretically predicted evolution (dashed line) and the simulation results (solid line) for the spot size

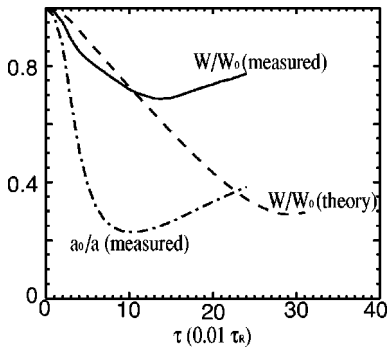

FIG. 1. Spot size evolution and intensity enhancement. Laser power $P=170$ TW, lens thickness $\Delta=1$ mm, and pulse length $L_0=57$ fs. Solid line: measured spot size; dashed line: theoretical value; dot-dashed line: a_0^{peak}/a^{peak}. Laser exits plasma at $\tau=0.0316\tau_R$.

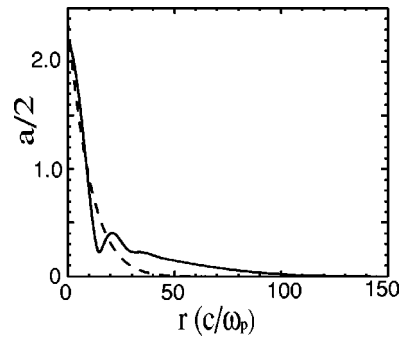

FIG. 2. Transverse lineout of normalized laser vector potential at peak intensity (solid line) and its Gaussian fit (dashed line), which shows that the distribution is non-Gaussian.

are plotted. For the simulation results the spot size is calculated at the axial position where the intensity is highest. As is clear there is a significant difference particularly outside the lens. The envelope equations predict a spot size reduction by a factor of 3 while the simulations show only a 30% reduction. This deviation was seen in each case listed in Table I. In addition, in the simulations the focal length of the lens is smaller than the theoretical estimates. In Fig. 1, it can be seen that the focal length in the simulation is half of the theoretical estimate. The reason for these discrepancies is twofold. The theory assumes that the transverse profile remains Gaussian and that the longitudinal profile remains fixed. In reality the transverse profile can become non-Gaussian from spherical aberrations in the lens and from Raman side scatter in the forward direction, while the axial profile can change from relativistic self-phase modulation and Raman forward scattering. These two effects also work in combination.

The spherical aberrations occur because for a Gaussian profile the focusing ''force'' does not vary linearly across the wave front. This is completely analogous with the the focusing of a particle beam in a plasma [27]. A parabolic, not a Gaussian, profile provides a perfect focusing lens. Those deviations from a perfect lens are called spherical aberrations. For a Gaussian pulse the rays at the outer edge are not focused strongly enough and higher-order Gaussian modes are generated. When analyzing the simulation data the spot size is defined as the second moment

$$W^2=\frac{\int_0^\infty rdra^2r^2}{\int_0^\infty rdra^2}.$$

So, if the portions of the beam at larger radii are focused more weakly than the average rate, then this weighted averaged spot size eventually becomes larger than that predicted by the theory. This is consistent with what was observed in Fig. 1.

Besides a reduction in spot size, another consequence of focusing is an increase in the normalized vector potential (or intensity) on the axis. If the laser beam's transverse profile remained Gaussian then these two would be proportional to each other. Therefore, a measure of the non-Gaussian nature of the beam is to see how the peak intensity scales with the weighted averaged spot size. In Fig. 1, the inverse of the peak intensity on the axis a_0^{peak}/a^{peak} is also plotted (dot-dashed line), which shows $a_0^{peak}/a^{peak}=0.23$ at the maximum peak intensity as compared to $W_{min}/W_0=0.72$. Notice also that the maximum peak intensity is reached (at $\tau=0.1\tau_R$) before the spot size focus (at $\tau=0.14\tau_R$). This shows that the different radial parts have different focal lengths. The beam center is focused more strongly and reaches the focus earlier than the beam edge. The non-Gaussian nature of the transverse profile is illustrated further in Fig. 2 where a transverse lineout of the laser amplitude at the maximum peak intensity is shown. For convenience a Gaussian fit is also shown.

The deviation from theory is not only due to spherical aberrations. As shown in Sec. II A, when the pulse length does not evolve the power is conserved at each axial position. However, in general the pulse can redistribute its energy axially, causing the pulse length to change and the local intensity to change even if the spot size remains fixed.

To study the pulse length evolution, we plot in Fig. 3 the pulse lengths from the simulation and the theoretical predictions of Eq. (2.22). The simulation pulse length is the second

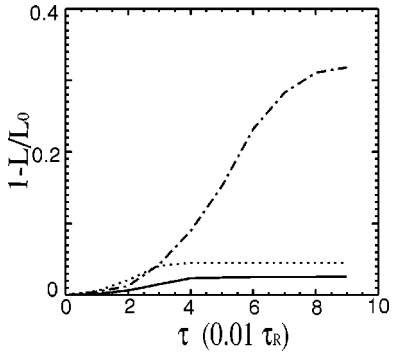

FIG. 3. Pulse length evolution. Solid line: $1-L/L_0$ from radially integrated intensity; dot-dashed line: that from the intensity on axis; dotted line: theoretical value. Laser exits plasma at $\tau=0.0316\tau_R$.

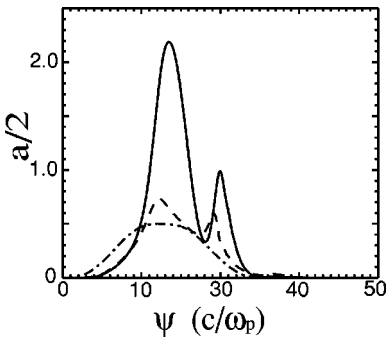

FIG. 4. Longitudinal distribution of normalized laser vector potential on axis at three different times, $\tau=0$ (dot-dashed line); $\tau=0.03\tau_R$ (dashed line); $\tau=0.1\tau_R$ (solid line). Laser exits plasma at $\tau=0.0316\tau_R$.

moment (similar to the spot size) of both the radially integrated intensity (solid line) and the intensity on axis (dot-dashed line). The length from the radially integrated profile is what the theory is calculated for and the simulation result agrees reasonably with the theoretical values. However, the beam center shows much more compression (dot-dashed line) than the theory and also continue to compress even outside the plasma, where the theory predicts no compression. This once again clearly demonstrates the non-Gaussian nature of the pulse. The change in pulse length along the axis indicates that different axial slices and different radial rings are each focused with different focal lengths. We also plot in Fig. 4 the laser intensity on axis at three different times. At $\tau=0.03\tau_R$, the pulse begins to develop an instability with a wavelength approximately $2\pi c/\omega_p$. This Raman type instability is another process causing longitudinal power transportation.

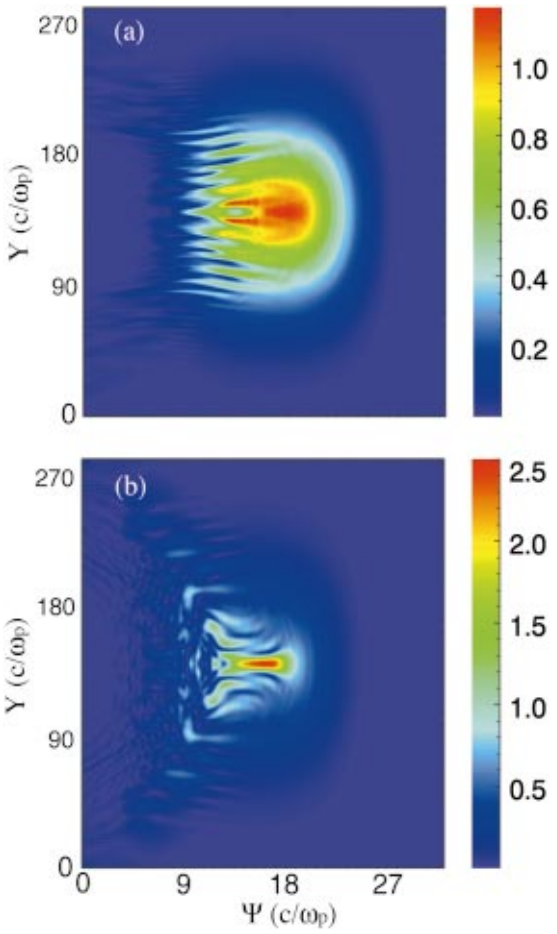

FIG. 5. (Color). Contours of the envelope of the normalized laser electric field from the OSIRIS simulation, $E(\tau=0)=1$. (a) $\tau=0.032\tau_R$, showing side scattering. (b) $\tau=0.07\tau_R$, showing focusing in the vacuum. Laser exits plasma at $\tau=0.05\tau_R$.

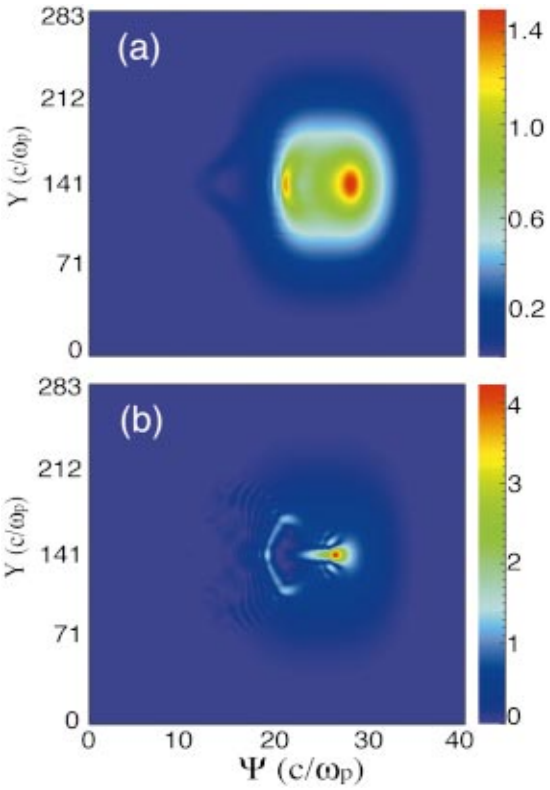

FIG. 6. (Color). Contours of the envelope of the normalized laser vector potential from the WAKE simulation, $a(\tau=0)=1$. (a) $\tau=0.031\tau_R$. (b) $\tau=0.063\tau_R$, showing focusing in the vacuum. Laser exits plasma at $\tau=0.05\tau_R$.

B. Raman instabilities

The Raman instabilities are complicated processes and different regimes often interact in a highly nonlinear fashion. In particular, backscattering, which is precluded in the envelope description of WAKE, can have an important effect. To better study the effect of the Raman instabilities, we use both WAKE and the fully explicit PIC code OSIRIS to simulate a pulse of $P/P_c=100$ and $L_{\mathrm{FWHM}}=45$ fs $(7.7c/\omega_p)$ passing through a lens with thickness of $\Delta=0.05z_R$ (1.7 mm). The simulation is done in a two-dimensional slab geometry.

The formulas in Sec. II D predict that the three-wave side scattering is dominant with an *e*-folding of 12.5 at the exit of the lens, while the gains for RFS and four-wave nonresonant RFS-SS are 5.3 and 2, respectively. Raman side scattering is clearly seen in the OSIRIS run of Fig. 5(a). (Note that in

OSIRIS the laser oscillations are explicitly resolved. In Fig. 5 only the laser envelope for the electric field is plotted.) However, after exiting the plasma, the pulse keeps focusing and reaches its focus outside the plasma [Fig. 5(b)]. Pulse compression is also evident. The contour of half maximum intensity has a width of $0.23W_0$ and a length of $0.56L_0$. The pulse diffracts beyond the focus. Since the instability causes the pulse to filament and hence to form an extremely non-Gaussian distribution, the analytical formulas derived in Secs. II A and II B, which are based on a Gaussian distribution, do not rigorously apply. Nevertheless, the enhancement of the intensity at the focus, $a_{max}^2/a_0^2 \approx 6$, is in line with the prediction of a spot size reduction of 6 given by Eq. (2.14).

For the same run, WAKE also shows similar instabilities [Figs. 6(a) and 6(b)]. Although the scattering part at the pulse back is not identical to the OSIRIS result, the picture at the pulse core looks similar (note that WAKE plots a while OSIRIS plots E). We suspect that the differences between the OSIRIS and WAKE simulations are due to the presence of backscattering in the OSIRIS simulation. For shorter and narrower pulses the two codes give very similar results. While the observed perturbations in Figs. 5(a) and 6(a) correspond to near forward side scattering which is, in principle, described by both codes, the perturbations in the OSIRIS simulation are larger. These perturbations must grow from some initial condition, which we suggest is seeded by the Raman backscattering. Although one normally thinks of backscattering as involving counterpropagating plane waves, examination of the OSIRIS simulations reveals that the backscattering occurs in radially localized regimes, which introduces radial structure to the laser pulse. The exact details depend on the initial temperature. This structure is the seed for the near forward side scattering. To test this idea we ran the WAKE code with a small transverse modulation applied to the initial laser pulse. The transverse wavelength of the modulations was selected to match the observed structure in the OSIRIS runs. We found that a perturbation as small as $\pm 2\%$ eventually grew and disrupted the main laser pulse. Thus, the Raman side scattering observed in the OSIRIS runs is consistent with the amplification of small perturbations.

We have given details for only a few illustrative examples. More examples of the cylindrically symmetric WAKE simulation results are summarized in Table I. For different laser power P_0, pulse length L_0, and plasma lens thickness Δ, we tabulate the separation between the focus and the lens exit $f-\Delta$, spot size reduction W_{min}/W_0, pulse length compression L/L_0, intensity enhancement $(a/a_0)^2$, and power enhancement P/P_0. The theoretical predictions for spot size reduction and pulse length compression are also listed.

IV. SUMMARY

We have derived analytical formulas for the spot size and pulse length evolution for a short laser pulse propagating in a thin uniform plasma lens. The formulas are compared to the simulation results from the PIC codes WAKE and OSIRIS. As predicted by the formula, the laser pulse can be focused outside the plasma. The simulations give a greater final spot size and a shorter focus than the formulas. The difference is mainly due to the transverse non-Gaussian distribution. To achieve a greater spot size reduction, a transversely nonuniform plasma lens is needed. Nevertheless, the simulations still predict a 30% spot size reduction at 3.3 mm away from a 1 mm plasma lens.

The simulation shows that Raman side scattering can develop when the pulse is inside the plasma. However, the Raman instabilities do not prevent the pulse from continuing to focus when it exits the plasma lens. This provides a way to experimentally prove relativistic self-focusing.

This work also indicates directions for future work. It would probably be of interest to consider different transverse profiles, i.e., profiles closer to a parabola shape, to try to reduce the spherical aberration. In addition, it might be of interest to use higher laser intensities. In the simulations, the initial value of a was kept at or below unity so that the weakly nonlinear theory would still marginally apply. However, using higher-intensity lasers might lead to less aberration since the nonlinearity saturates on axis.

ACKNOWLEDGMENTS

This work was supported by DOE Contract No. DE-FG03-98DP00211, NSF Grant No. DMS 9722121, and LLNL under contract No. W-7405-ENG-48 (at UCLA); by DOE Contract No. DE-FG03-92ER40745 (T.K.); and by DOE Contract No. DE-FG02-97ER41039 and NSF Grant No. THY9722158 (T.A.).

[1] E. Esarey, P. Sprangle, J. Krall, and A. Ting, IEEE Trans. Plasma Sci. **24**, 252 (1996), and references therein.

[2] Special issue on *Generation of Coherent Radiation Using Plasmas*, edited by W. B. Mori, special issue of IEEE Trans. Plasma Sci. **PS-21**, 1 (1993), and references therein.

[3] W. B. Mori, IEEE J. Quantum Electron. **33**, 1942 (1997), and references therein.

[4] A. G. Litvak, Zh. Éksp. Teor. Fiz. **57**, 629 (1969) [Sov. Phys. JETP **30**, 344 (1970)].

[5] C. Max, J. Arons, and A. B. Langdon, Phys. Rev. Lett. **33**, 209 (1974).

[6] P. Sprangle, C. M. Tang, and E. Esarey, IEEE Trans. Plasma Sci. **PS-15**, 145 (1987).

[7] G.-Z. Sun, E. Ott, Y. C. Lee, and P. Guzdar, Phys. Fluids **30**, 526 (1987).

[8] X. L. Chen and R. N. Sudan, Phys. Rev. Lett. **70**, 2082 (1993).

[9] E. Esarey *et al.*, IEEE J. Quantum Electron. **33**, 1879 (1997), and references therein.

[10] C. J. Mackinstrie and R. Bingham, Phys. Fluids B **4**, 2626 (1992).

[11] A. B. Borisov *et al.*, Phys. Rev. Lett. **68**, 2309 (1992); P. Monot *et al.*, *ibid.* **74**, 2953 (1995); R. Wagner *et al.*, *ibid.* **78**, 3125 (1997); K. Krushelnick *et al.*, *ibid.* **78**, 4047 (1997); C. E. Clayton *et al.*, *ibid.* **81**, 100 (1998).

[12] T. M. Antonsen, Jr. and P. Mora, Phys. Rev. Lett. **69**, 2204 (1992); Phys. Fluids B **5**, 1440 (1993).

[13] P. Chen, Part. Accel. **20**, 171 (1987).
[14] T. Katsouleas, J. J. Su, W. B. Mori, and J. M. Dawson, Phys. Fluids B **2**, 1384 (1990), and references therein.
[15] P. Mora and T. M. Antonsen, Jr., Phys. Plasmas **4**, 217 (1997).
[16] H. G. Hemker, Ph.D. thesis, University of California, Los Angeles, 2000.
[17] *The Supercontinuum Laser Source*, edited by R. R. Alfano (Spring-Verlag, New York, 1989).
[18] G. P. Agrawal, *Nonlinear Fiber Optics*, 2nd ed. (Academic Press, San Diego, 1995).
[19] E. Esarey *et al.*, Phys. Rev. Lett. **84**, 3081 (2000).
[20] B. Hafizi *et al.*, Phys. Rev. E **62**, 4120 (2000).
[21] D. Anderson and M. Bonnedal, Phys. Fluids **22**, 105 (1979).
[22] B. J. Duda, R. G. Hemker, K.-C. Tzeng, and W. B. Mori, Phys. Rev. Lett. **83**, 1978 (1999); B. J. Duda and W. B. Mori, Phys. Rev. E **61**, 1925 (2000).
[23] K.-C. Tzeng and W. B. Mori (unpublished).
[24] In Refs. [20] and [23], fully nonlinear equations for the spot size evolution (valid for any a) are derived: $\ddot{W}=4/(k_0^2W^3)(1-(2W^2\omega_p^2/Ic^2)\{\sqrt{1+I}-1-\ln[(1+\sqrt{1+I})/2]+\sqrt{1+I}-1\}+[\ln(1+I)/I-1])$, where $I=a^2/2$ for the linear polarization considered here. The last term is from ponderomotive blowout, which can be neglected when spot size is large. Expanding the remaining terms, we can see the next term is $a^2/3$ times smaller than the leading term kept in our paper.
[25] P. Sprangle, A. Ting, and C. M. Tang, Phys. Rev. A **36**, 2773 (1987).
[26] C. D. Decker, W. B. Mori, T. Katsouleas, and D. E. Hinkel, Phys. Plasmas **3**, 1360 (1996), and references therein.
[27] J. J. Su, T. Katsouleas, J. M. Dawson, and R. Fedele, Phys. Rev. A **41**, 3321 (1990).